RSC Advances

ROYAL SOCIETY
OF CHEMISTRY

www.rsc.org/advances

Journal Name

ARTICLE

Highly Organized Nanofiber Formation from Zero Valent Iron Nanoparticles after Cadmium Water Remediation

Keyla T. Soto[a,b], Rolando Guzmán-Blas[c], Edwin O. Ortiz-Quiles[c], Estevão Rosim Fachini[d], Juan Corchado-García[c], Eduardo Larios[e,f], Beatriz Zayas[g], Miguel José-Yacamán[e], and Carlos R. Cabrera[c*]

Many studies have used nanoscale zero valent iron (nZVI) nanoparticles to remove redox-sensitive metals (e.g., As, Cr, U, Se, Ni, Cu) from aqueous systems by absorption or reduction processes. However, very few investigations present a detailed study of the product formed after remediation process. In order to quantify the efficiency of nZVI particles as a possible cadmium remediation agent, we prepared nZVI by sodium borohydride reduction of an iron complex, $FeCl_3 \cdot 6H_2O$, at room temperature and ambient pressure. Fe^0 and nanocrystalline structures of iron oxides and oxyhydroxides were obtained with this method. We exposed the nZVI to 6 ppm of Cd^{2+} and characterized the products with X-ray Diffraction, X-ray Absorption and X-ray Photoelectron Spectroscopy. Inductively coupled plasma analysis showed that the nZVI remediation efficiency of cadmium ions was between 80% and 90% in aqueous media. All of the physical characterization results confirmed the presence of Fe^0, α-Fe_2O_3 and FeOOH. High resolution transmission electron microscopy images showed nanofiber formation of a mixture of Fe^0, oxyhydroxides and oxides iron formed after interacting with Cadmium ions, possibly forming $CdFe_2O_4$. These results suggest that the FeOOH shell and other iron oxides in nZVI could enhance Cd^{2+} removal. This removal is observed to cause a change of the initial structure of nZVI to nanofibers due to possible formation of $CdFe_2O_4$ as a waste product.

A. Introduction

Cadmium is a metal used today by industry (e.g. electronic industry) that has been released to the environment through the combustion of fossil fuels, metal production, use of phosphate fertilizers, electroplating, and the manufacturing of batteries, pigments, and computer screens.[1] This metal tends to accumulate in plant and animal tissues, reaching dangerous levels in the food chain, even when released in small amounts.[2,3,4] Cadmium is toxic at high concentrations because it disrupts enzyme functions, replacing essential metals in pigments or producing reactive oxygen species.[5] It is poorly retained by the soil and is readily absorbed by plants.[6,4,2] This heavy metal can be accumulated in leaves and cause phytotoxic effect on plants, such as chloroplast structure change and cell death.[7,8] In hazardous waste sites, the levels of cadmium in the soil has become about 4 parts per million, while in water the levels have reached 6 ppm.[9]

U.S. Environmental Protection Agency (EPA) recognize cadmium to be a probable human carcinogen (e.g. breast cancer) and has been classified as a Group B1 carcinogen.[9,10,11] Since cadmium represents a great threat to human health, considerable effort has been placed on the development of techniques to remove this contaminant from water.[12]

In the course of developing suitable options to treat heavy metal contaminants in wastewater, nanoscale zero valent iron (nZVI) particles have been found to be an alternative approach to reduce the concentration of several kinds of contaminants.[13,14] This approach provides a real alternative to remove cadmium by using particles at nanoscale. Cadmium remediation is of the utmost importance because Cd species have been detected in aquatic ecosystems and found to bioaccumulate in organisms in nanomolar to micromolar concentrations.[2] Iron nanoparticles are particularly attractive for remediation purposes due to their significant surface area to mass

ratio, leading to a greater density of reactive site and heavy metal removal capacity.[14] Because of their smaller size, nanoscale based iron materials are much more reactive than conventional iron powders and they can be easily suspended in slurry and pumped straight to the contaminated site.[15,16] Efficient nZVI remediations of groundwater contaminants have been shown in multiples studies.[17,18,19,20,12] However, in the literature there is a lack of comparable studies for different nZVI materials and deployment strategies.[13]

Very few investigations of nZVI materials present a detailed study of the products formed in the remediation process. Various adsorption and kinetic models to describe metal adsorption on nZVI and Cd-nZVI surfaces using SEM/EDX and XPS measurements have been studied[1,13] but, to our knowledge, the interactions between surface Fe(0) and Cd (II) and subsequent cadmium retention in nZVI particles has not been the subject of detailed study. The specific objectives of this work are to 1) analyze by Inductively Couple Plasma measurements the efficiency of the nanoscale zero valent iron (nZVI) at low treatment dose in the removal of Cd(II); 2) characterize the nanoparticles of Fe^o, Fe^o-H_2O and Fe^o-Cd using spectroscopy and microscopy techniques; and 3) establish a conceptual model of the Cd ions with the surface of nZVI. Results from this study provide important information of the products formed during the remediation process of cadmium. We also report an unexpected nanofiber formation and the potential synthesis of cadmium ferrite. This remediation product has been suggested as a photocatalyst material that has tremendous potential application for light harvesting.[21] These results could be useful because by understanding the products of remediation processes, alternative applications may be suggested for them. This will decrease the amount of new toxic substances formed after water remediation processes.

B. Experimental

B.1. *Chemicals*

The chemicals used were iron (III) chloride hexahydrate (97%, ACS reagent), sodium borohydride (≥98.5%, reagent grade), trichloroethylene (99.5+%, ACS reagent), Tween® 80 and humic acid (sodium salt) obtained from Sigma-Aldrich, $FeCl_3 \cdot 6H_2O$ (F2877 Sigma Aldrich), $NaBH_4$ (Alfa Aesar), ethanol 200 proof, 99.5% anhydride (Sigma Aldrich), Cd $(CHOO_3)_2$. 2 H_2O (Sigma Aldrich) and HCl (Alfa Aesar). All solutions were prepared with deionized water (18.2 MΩ-cm, Nanopure Diamond, Barnstead).

B.2. *Preparation of nanoscale zero valent iron*

Nanoscale zero valent iron (nZVI) particles were produced by adding $NaBH_4$ as the reducing agent to a solution of $FeCl_3 \cdot 6H_2O$. The resulting reductive reaction may be given as:[22]

$$2\ Fe^{3+} + 6\ BH_4^- + 18\ H_2O \rightarrow 2\ Fe^0(s) + 6\ B(OH)_3 + 21H_2 \quad (1)$$
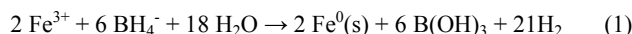
To obtain 1.13 g of nZVI, a 0.6 M solution of $FeCl_3$. $6H_2O$ (molar mass 270.30 g/mol) was prepared in 30 mL of ethanol (83% v/v) and nanopure water (17% v/v). The solution was purged with N_2 for 30 minutes to remove oxygen prior to the reaction; this was done to avoid the rapid oxidation of iron. Then, the solution was titrated by adding a total of 100 mL of 0.8M $NaBH_4$ aqueous solution under a nitrogen atmosphere.

After 30 minutes of stirring with a magnetic bar at 700 rpm, the solution was filtered using a 0.22 μm filter paper (Millipore) under vacuum at 25 °C.

The sample was rinsed three times with 99% absolute ethanol. Various filtered samples, prepared as mentioned, were placed immediately in a vacuum desiccator.

B.3. *Preparation of Cadmium concentrations in synthetic wastewater*

Cadmium solutions were prepared using $Cd(CH_3COO)_2$. $2H_2O$ due to its high solubility in water and ethanol. To represent different samples of wastewater contaminated with cadmium, a solution of 6 ppm was prepared. This was followed by two dilutions of the 6 ppm solution (stock concentration) to prepare solutions of 3 ppm and 1 ppm. The initial pH of each solution was adjusted to 2 using 1.0 M HCl. Concentration units were presented as "ppm" in keeping with toxicity nomenclature (ppm = mg/L)

B.4. *Determination of the reduction of the cadmium concentration in aqueous solution nZVI*

All reactions were carried out in a dry box under argon atmosphere to prevent Fe oxidation. In some treatment processes with 1 ppm or more of Zn (which has chemical properties similar to Cd) the dose used was between 1.0g/L to 3.5g/L of nZVI.[23] Here, 200 mL of all the prepared cadmium solutions of 1, 3 and 6 ppm were treated with 3.0 g/L of nZVI in periods of 1, 3, and 5 hours. One sample of each solution was taken before and after treatment to corroborate the accuracy in the preparation of the initial concentrations and to determine the final concentration of cadmium.

The pH of each cadmium solution was determined before and after adding the nZVI. To determine the effect of the nanoparticles in the amount of cadmium ions in the samples after certain reaction time, the samples were processed and analyzed using inductively coupled plasma (ICP-AES) Model: Perkin Elmer 4300 DV with a detection limit of 0.002 ppm for cadmium.

C. Results and discussion

C.1. *Characterization of Fe^0, Fe^0/H_2O and $Fe^0/$ Cd particles*

Characterization of nZVI is needed to understand their reaction mechanism and kinetics.[18] In this study, the synthesized nanoparticles and nanofibers were characterized by X-Ray Photoelectron Spectroscopy (XPS), X-Ray Absorption (XAS), High Resolution Transmission Electron Microscopy (HRTEM) and X-Ray Diffraction (XRD).

HRTEM images were done with a Cs-corrected JEOL JEMARM200F electron microscope operated at 200 kV and equipped with a CEOS Cs corrector on the illumination system. XRD patterns were obtained on a PANalytical X'Pert Material Research Diffractometer operating with a Cu Kα radiation (λ=1.54 Å) source. XPS binding energy spectra were obtained using a PHI spectrometer equipped with an Al Kα mono and polichromatic X-ray source operating at 15 kV, 350 W and pass energy of 58.70 eV. All the binding energies reported were corrected fixing the carbon 1s peak (C 1s) at 284.5 eV. X-ray absorption spectroscopy (XAS) was carried at National Synchrotron Light Source (NSLS) in Brookhaven National Laboratory (BNL) using beam line X18A. The iron K edge (7112 eV) was measured for the Cd-nZVI sample in transmission mode. The data acquisition setup consisted of three 12 in. ionization chamber detectors: Incidence (I_0) Transmittance (I_T) and reference (I_{Ref}) detector.

Data analysis was done with the Demeter Suite of Programs.[24] The Athena software was used for linear combination fittings of the X-Ray Absorption Near Edge (XANES) region with theoretical XANES spectra of different iron species. The reference spectra were calculated with the Hephaestus program.

C.2. *Analysis of reduction process in cadmium concentration after treatment with Fe^0 nanoparticles*

Previous researchers have studied redox and adsorption processes as mechanisms of metal concentration reduction by nanoscale iron.[15] However, there is very little research that presents in detail adsorption features that occur with certain metals (i.e. cadmium).[13] Iron nanoparticles have standard a reduction potential (E°) of - 0.447 V, which is lower than the reduction potential of cadmium (-0.40V, 25°C).[1,13] Similar with other studies, our data suggest that Cd^{+2} is sequestered on nZVI by adsorption or surface complex formation with no apparent reduction of Cd^{+2}.[25]

To analyze the results and determine the concentration reduction of cadmium in the nZVI sample, we used ICP. According to the results, we observe a change in the decrease of cadmium concentration as treatment time elapsed. The maximum percentages of cadmium adsorption relative to the initial concentration (% C_{Cd}) for Cd^{+2} aqueous solutions of 1, 3 and 6 ppm were 93%, 91% and 89%, respectively (see **Figure 1**). These percentages were obtained in a period of 5 hours, which indicates that longer interaction times between cadmium ions and nZVI promoted larger cadmium concentration reduction.
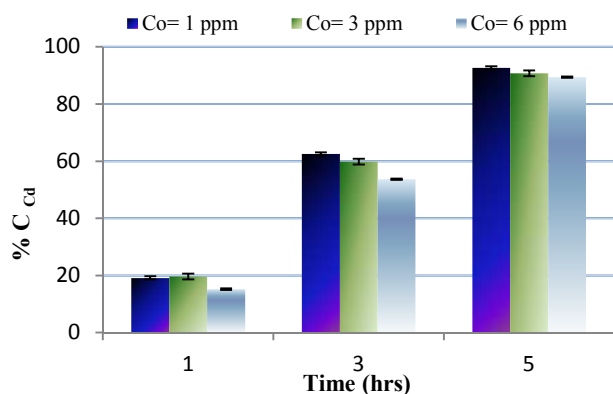

Figure 1. Bar graph of the ratio between final and initial cadmium (II) ion concentration (C $_{Cd}$) versus time. The nZVI concentration (C_{Fe}) was 3 g·L^{-1} and cadmium concentrations (C$_0$) were 1, 3 and 6 ppm. Experimental conditions: pH= 2; 25°C; argon atmosphere; magnetic bar stirrer at 700 r·min^{-1}.

The correlation between the final concentration versus time and the coefficient of determination (R^2) for the three concentrations was calculated. The correlations for the 6 ppm, 3 ppm, and 1 ppm Cd^{2+} samples gave values of 0.944, 0.989 and 0.992, respectively. These values indicate that the percentage of the variability of the final cadmium concentration may be proportional with respect to reaction time. Nevertheless, for the 6 ppm Cd^{2+} sample, there seems to be an induction period until the pH reaches a value higher than 4 when the rate of adsorption increases and reaches the same rate as the 3 and 1 ppm samples after 3 hours.
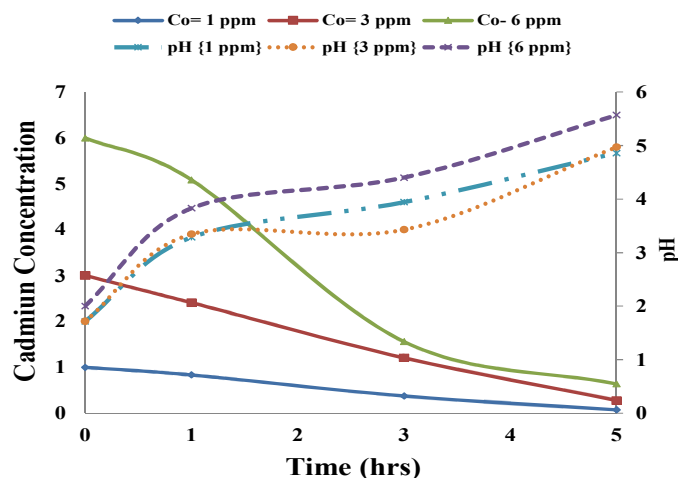

Figure 2. Correlation of the final cadmium concentration and solution pH vs. time using nZVI with initial pH of 2 and C_{Fe}= 3 g·L^{-1}; Initial Cd^{2+} concentrations of 1, 3, and 6 ppm; temperature of 25°C and under argon atmosphere; magnetic bar stirrer was at a *w* of 700r·min^{-1}.

The samples showed changes of pH from 2 to 6 with increasing cadmium treatment time. This is due to the formation of hydroxides (OH-) on the surface of the nZVI by its interaction with water.[23] The maximum cadmium reduction efficiency was greater in 5 hours of treatment. Previous studies suggested that the rate and efficiency in metal reduction increases as the pH decreases.[25] When water has a basic initial pH, iron may precipitate as an oxyhydroxide. The presence of this elements cause a passivation on the surface of the iron nanoparticles. Thus, acidic pHs should be used for best results.[23]

These studies prove that nZVI are a viable option in order to decrease cadmium contamination in affected sites. Since cadmium is being removed from the solution, it must mean that the nZVI plays a role in cadmium sequestering. Thus, it is expected that the used nZVI contains cadmium, which would in turn make the remediation product toxic. For this reason, we decided to analyze the structure of used nZVI in order to gain an understanding of the interactions between nZVI and cadmium. This new knowledge may serve to optimize the remediation process and to provide alternatives uses for the remediation product.

C.3. *X-ray photoelectron spectroscopy analysis*

In the XPS spectrum, we observed binding energy peaks for Fe 2p$_{3/2}$ and O1s of the prepared nanoparticles (**Figure 3.A**). The XPS spectrum also shows peaks for oxygen, iron and adventitious carbon (from atmosphere contamination). The amount and extension of rinsing was determined following the presence or absence of B1s and Na1s peaks at the XPS spectrum. Rinsing in this synthesis procedure is a critical step, necessitating the use of absolute alcohol, because water promotes rapid oxidation when the samples are exposed to the atmosphere.[26] Cd-nZVI particles were analyzed by high resolution XPS to determine the elemental composition and the valence state of elements on the nZVI surface.

The Fe 2p$_{3/2}$ peak in the XPS spectrum for elemental iron commonly arises at 707 eV.[27] The Fe 2p$_{3/2}$ peak located at 711 eV was ascribed to ferric iron.

Since the major contribution on the Fe $2p_{3/2}$ envelope from a fresh iron nanoparticles sample corresponds to Fe(III) (see **Figure 3.B**), the particles should have a core of metallic iron surrounded by a thick outer shell of iron oxides/hydroxides. Probably this oxygenated iron layer was rapidly formed after the particles had been exposed to the atmosphere. The FWHM for the Fe^{III} $2p_{3/2}$ peak in the XPS spectrum was large (4.0 eV) which also \suggests multiple oxidized species of iron on the surface

This interpretation is compatible with the XPS spectrum for the oxygen that presented great amounts of metal oxides (530.0 eV, 41%) and metal hydroxides (531.5 eV, 57%) species, as determined by deconvolution treatment on the O1s binding energy peak (data not shown). The O1s peak also indicates that water was practically absent on the surface, since any significant contribution (less than 2 %) was found for the O1s peak at binding energies higher than 533 eV. Examining the ratio of peak areas Fe/OH and OH/O²⁻ it was established that the covering oxide layer may be composed of iron hydroxides or oxyhydroxides. This is an important observation because the mechanism for aqueous metal contamination adsorption is regulated by the presence of different oxygenated groups on the particle surface. A number of mechanisms have been proposed, depending also of the adsorption conditions such as pH and the kind of metal ion that is being fixed on the surface.[26,27,28]. The binding energy difference between Fe $2p_{3/2}$ and Fe $2p_{1/2}$ was 13.6 eV, making the assignment of the principal iron specie as Fe^{III} in Fe_2O_3 and FeOOH.[28]

In the XPS spectrum, metallic iron was only identified in fresh samples (see **Figure 3.B**). After approximately 12 months aging, little or any presence of the zero valence iron could be determined (see **Figure 3.C**).

The arrows in the spectra indicate the Fe 2p satellites contribution, which are characteristic of Fe (III) state. The spectrum also suggests small amounts of Fe (II) for freshly prepared nanoparticles, since a small shoulder can be seen in Figure 3.b at 729 eV. This is because iron reacts not only with the contaminants, which are generally present at low concentrations, but also with dissolved oxygen and with water as shown below.[29]

$$2Fe^0(s) + O_2(g) + 4H^+ \rightarrow 2Fe^{2+}(aq) + 2H_2O(l) \quad (2)$$

$$Fe^0(s) + 2H_2O \rightarrow Fe^{2+}(aq) + H_2(g) + 2OH^-(aq) \quad (3)$$

Through a high resolution XPS, Cd $3d_{3/2}$ and $3d_{5/2}$ peaks can be observed (**Figure 3.D**). After completing the deconvolution of the peaks, a Cd^{2+} signal can be detected, especially at 405 eV which is in accordance with the values reported for in the literature [13]. The XPS results confirm the ICP data; the reduction of cadmium concentration on the test solutions is due to nZVI. Data suggest that Cd^{+2} is sequestered within nZVI by adsorption or surface complex formation with no apparent reduction on the nZVI surface.

C.4. *XAS analysis*

Figure 4. XANES region of the XAS measurements of the Cd-nZVI particles with the theoretical linear combination peak with reference spectra of Fe⁰, Fe_2O_3, Ferrihydrite and FeO(OH).
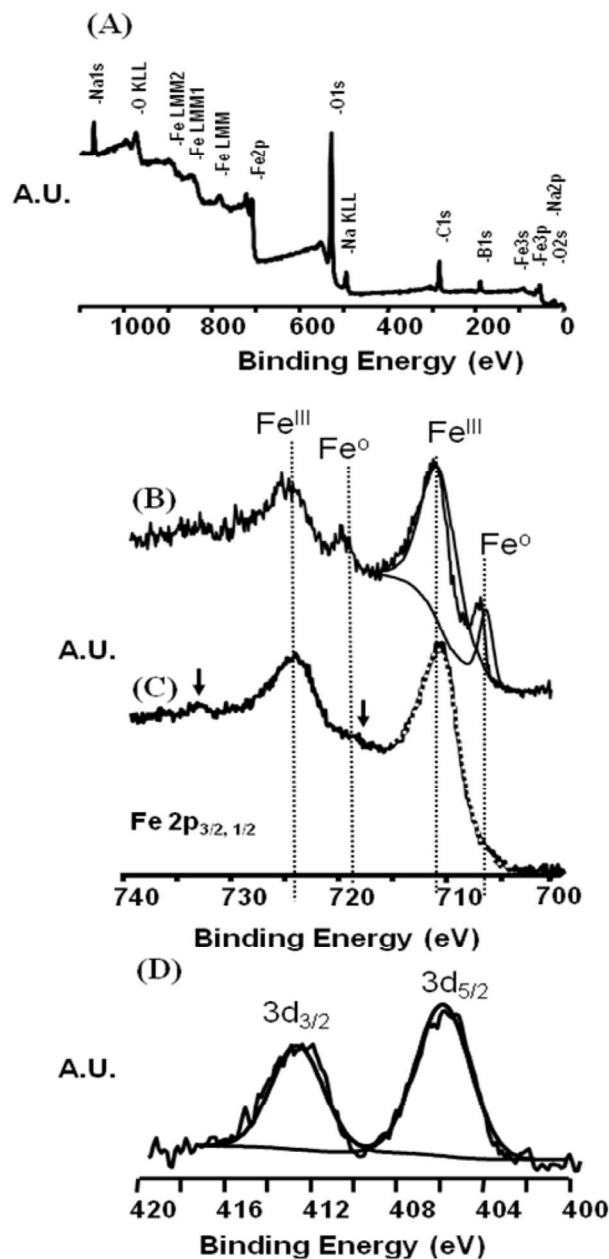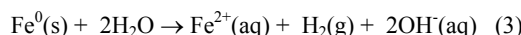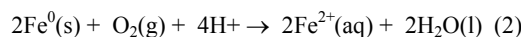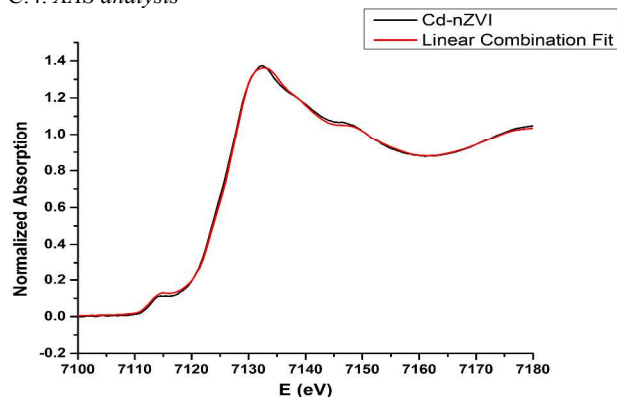
Figure 3. X-ray photoelectron spectroscopy spectrum of nZVI particles (A) and spectra of the Fe 2p binding energy region for (B) freshly synthesized and (C) one year old, under dry air, of nZVI particles. (D) spectra of the Cd 3d binding energy region for the samples of nZVI particles exposed to 6 ppm Cd^{2+} aqueous solution (3 g·L⁻¹ of nZVI, contact time of 5 h).

XPS studies confirmed the presence of both cadmium and oxygen containing iron species on the nZVI surface. Due to the limitations of the surface sensitive XPS technique, XAS experiments were performed because they can provide a better understanding of the bulk composition of the various oxygen containing iron species[30,31]. The linear combination fit was done in the 7092 eV and 7142 eV range of the sample spectrum and the theoretical spectra. The fit was done with reference spectra of Fe^0, Fe_2O_3, Ferrihydrite, FeO(OH) and γ-FeO(OH). 25 different combinations of the 5 reference spectra were performed and the model with the least residual error was chosen.

Iron Species	Composition %
Fe^0	23%
α-Fe_2O_3	17%
Ferrihydrite	47%
FeO(OH)	13%
γ-FeO(OH)	0%

Table 1. Composition of the Cd-nZVI sample derived from linear combination fitting of the XANES sample spectrum with reference spectra of Fe^0, Fe_2O_3, Ferrihydrite, FeO(OH) and γ-FeO(OH).

Figure 4. shows that a good fit was achieved with the reference spectra used and **Table 1.** summarizes the percent composition results. The predominant oxygen containing iron species in the Cd-nZVI sample were ferrihydrite and α-Fe_2O_3 which is consistent with the XPS analysis. This implies that ferrihydrite and α-Fe_2O_3 can be found both in the surface of the sample and in the bulk. The linear combination fitting detected the presence of metallic iron in the Cd-nZVI sample whereas the XPS shows almost no metallic iron signals. The apparent contradiction between XPS and XAS can be explained by the fact that the metallic iron contained in the samples is covered by and oxidized iron layer. The surface sensitive XPS technique cannot detect it but the bulk sensitive XAS technique can. This sugests that the structure of the Cd-nZVI may contain an Fe^0 core surrounded by a shell made up of ferrihydrite and α-Fe_2O_3. This hypothesis is confirmed by HRTEM studies discussed later. The presence of α-Fe_2O_3 throughout the bulk is particularly interesting because studies show that $CdFe_2O_4$ is formed under similar conditions as those in this study when α-Fe_2O_3 is in the presence of Cd^{2+}. In order to confirm the formation of $CdFe_2O_4$, XRD and HRTEM studies were performed.

C.5. *X-ray diffraction patterns*

Three XRD patterns with broad peaks characteristic of small particles are shown in **Figure 5**. In **Figure 5.A**, a nZVI sample pattern with two peaks at 44.9° and 65.1°, which indicate the presence of body-centered cubic crystal Feº, is presented. Both peaks are in good agreement with those reported in the literature[32,33,34,35]. In the next pattern (**Figure 5.B**), nZVI were placed in water for 5 hours as a blank to compare the oxidation states without the presence of cadmium. The intensity of the characteristic peak for Fe^0 near 44.9° decreases in this pattern. A possible explanation to this change is a strong interaction of the iron with the oxygen either from the atmosphere at the time of preparation or the hydroxides (OH-) group from the water. Preliminary results indicate that these iron nanoparticles can prevent oxidation under atmospheric conditions for extended periods[22,18,21]. Characteristic peaks of hematite (α-Fe_2O_3) were identified.[36] Xiaoqin Li et al. also proves the formation

of Fe_2O_3 and FeOOH in a previous work.[37,30]

In this work, we obtained similar peaks of α-Fe_2O_3 and FeOOH visible at 30.2°, 38.0°, 43.3°, 49.1°, 57.2° and 62.8°; and 27.1°, 35.6°, 46.9°, 52.9° and 60.6°, respectively.
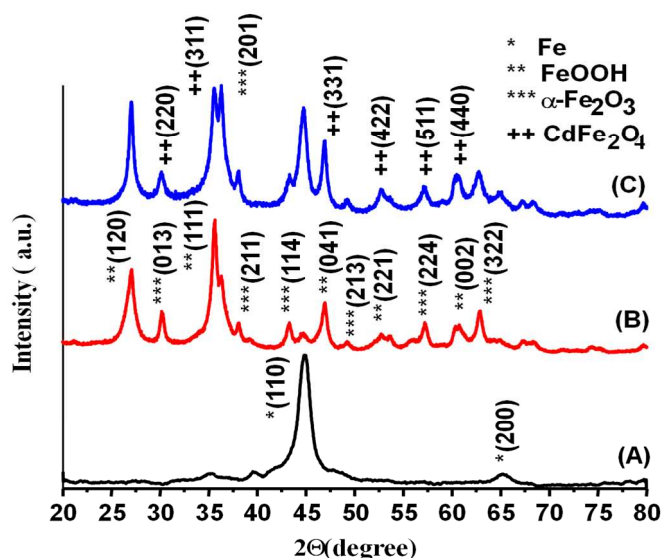

Figure 5. X-ray diffraction pattern of nZVI particles synthesized using the sodium borohydride reduction method. (A) pure nZVI particles freshly synthesized; (B) nZVI particles exposed to nanopure water (3 g·L^{-1} of nZVI, contact time of 5 h) and (C) nZVI particles exposed to 6 ppm Cd^{2+} aqueous solution (3 g·L^{-1} of nZVI, contact time of 5 h)

In **Figure 5.C**, an XRD pattern of nZVI at 3 g·L^{-1} placed for 5 hours with 6 ppm of Cd^{2+} is presented. This pattern has several peaks that required a comprehensive analysis. Previous studies show that $CdFe_2O_4$ may occur in similar chemical environments as the one presented in this work. **Figure 5.C** due to the low amount of cadmium used during the preparation of the sample. A pattern analysis was completed and characteristic peaks were identified for Fe^0: 44.7° and 65.0°; α-Fe_2O_3: 36.3°, 38.2°, 43.2°, 49.1° and 62.7°; FeOOH: 27.1°; and $CdFe_2O_4$: 30.1°, 35.6°, 46.9°, 52.6°, 57.1° and 60.6°.[38,21] Diffraction lines of Fe_2O_3 in the XRD pattern of nZVI exposed to Cd indicates that possible formation of $CdFe_2O_4$ is partial.[39] This analysis was done taking in consideration that possible $CdFe_2O_4$ formation can occur at different temperatures based on previous works.[39,40,41]

An important observation is the nZVI peak in 44.7º has a higher intensity in **Figure 5.C** than in **Figure 5.B**. The change in intensity may be explained as a result of cadmium interacting with oxygen. This reaction prevents iron to have enough oxygen available to fully react with it, preserving metallic iron integrity. In general, intensity changes of all peaks are observed in both samples (**Figure 5.B and 5.C**), suggesting different physical arranges after the cadmium exposure to nZVI. These results can be explained by a strong interaction between the Fe (III), O and Cd (II) detected in the XPS results, probably by the formation of cadmium ferrite.

The mean crystallite size (L) of nZVI samples can be calculated by using Scherrer's equation[42]:

$$L=0.9\lambda/(B_{2\Theta}\cdot\cos(2\Theta)) \qquad (4)$$

where λ is the wavelength of the X-ray (1.540 56 Å), 2θ is the angle at the maximum of the peak, and $B_{2\theta}$ is the width of the peak at half-height.

The pure iron standard had a Fe^0 particle size of 7.7 nm, the Fe^0- H_2O sample, where we observe Fe_2O_3, FeOOH and small quantities of Fe^0, had a particle size of 16.6 nm. The samples with Fe^0-Cd, where FeOOH, Fe_2O_3, Fe^0 are clearly observed and possible formation of $CdFe_2O_4$ was identified, had a particle size of 12.4 nm. The observed decrease in the average particle size of the samples with the possible formation of $CdFe_2O_4$ with respect to samples of Fe_2O_3 and iron oxides is referred to the strong chemical affinity of Cd^{+2} to the tetrahedral A site and the metastable cation distribution in the nanoscale range of the ferrites particles. [46] These chemical characteristics can help explain that there is a dependence of particle size with the stoichiometry of the cations.

C.6. High Resolution Transmission Electron Microscopy

HRTEM images of synthesized iron nanoparticles exhibit spherical shapes and chain aggregates (see **Figures** 6.A and **6.B**) as shown by others.[43] These images show that the particles have a diameter range between 25 nm and 64 nm. The aggregates may be due to the magnetic properties of Fe^0, which promotes iron linear orientation.[44,45,46]

The pure iron standard had an Fe^0 particle size of 7.7 nm, the Fe^0- H_2O sample, where we observe Fe_2O_3, FeOOH and small quantities of Fe^0, had a particle size of 16.6 nm. The samples with Fe^0-Cd, where FeOOH, Fe_2O_3, Fe^0 are clearly observed and possible formation of $CdFe_2O_4$ is identified, had a particle size of 12.4 nm. The observed decrease in the average particle size of the samples with the possible formation of $CdFe_2O_4$ with respect to samples of Fe_2O_3 and iron oxides is referred to the strong chemical affinity of Cd^{+2} to the tetrahedral A site and the metastable cation distribution in the nanoscale range of the ferrites particles. [46] These chemical characteristics can help explain that there is a dependence of particle size with the stoichiometry of the cations.
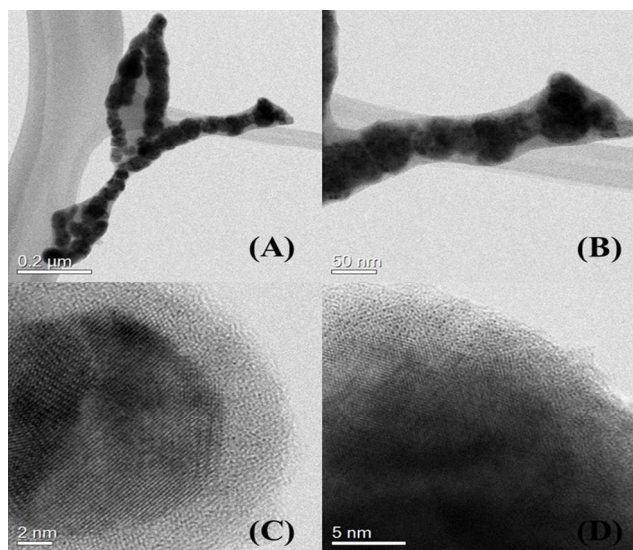

Figure 6. Transmission electron microscopy images of nZVI particles after suspension in pure water. Experimental conditions: nZVI particles concentrarion of 3 g.L^{-1}; pH adjusted to 2 with dilute solution of HCl, temperature at 25°C, argon atmosphere; 5 hours; magnetic bar stirrer at 700 r·min^{-1}.

The HRTEM images (see **Figures 6.C** and **6.D**) show a core-shell structure where the core is Fe and the shell may be iron oxides such as FeOOH, α-Fe_2O_3 (see **Figure 6.B**). The HRTEM images of the Cd^{+2} treated nZVI show nanofiber formation (see **Figure 7**), while the HRTEM images of untreated nZVI samples do not present nanofibers, only clusters and nanoparticles.
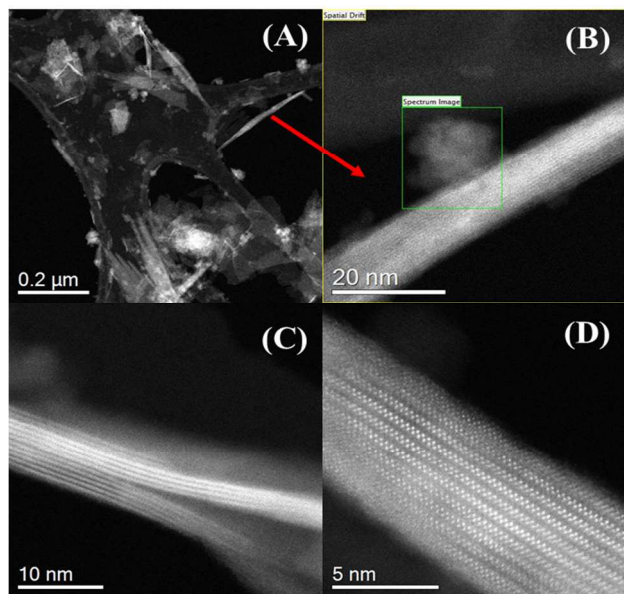

Figure 7. High resolution transmission electron microscopy of iron nanofibers formed during the cadmium ion remediation process. The contact time was 5 h, the nZVI concentration (C_{Fe}) was 3 g.L^{-1}; and Cd(CH$_3$COO)$_2$·2H$_2$O concentration (C$_0$) was 6 ppm. Experimental conditions: pH= 2; 25°C; argon atmosphere; magnetic bar stirrer at 700 r·min^{-1}.

The presence of two nano-constituents in the core-shell structure may impart dual properties for contaminant removal: the metallic iron acts as the electron source and exerts a reducing character, while the oxide shell facilitates the sorption of contaminants via electrostatic interactions and forming complexes with the surface. At the same time, the oxide shell allows electron passage from the metal core.[47]

A structural model of Cd -nZVI fibers is illustrated in Figure 8. We proposed this conceptual model of Fe^0(nZVI), FeOOH / α-Fe_2O_3 and $CdFe_2O_4$/α-Fe_2O_3/ FeOOH nanofibers considering the results of XRD patterns, XPS, XAS and HRTEM images. Figure 8.A shows the Fe^0 nanoparticles, Figure 8.B shows the Fe^0- H_2O where we observe Fe_2O_3 and FeOOH surrounding small quantities of Fe^0 and 7.C shows Fe^0-Cd where we observe $CdFe_2O_4$, FeOOH, Fe_2O_3 and Fe^0. In the case of the formation of the structure of Figure 8C, cadmium ions act as the limiting reagent, where the onset of the reaction of Cd, Fe^0, Fe_2O_3 and FeOOH allowing the possible formation of cadmium ferrite. Henceforth, the structure changes detected by HRTEM are consistent with the presence of Cd ions in the sample as presented in XPS and XRD studies.

The oxyhydroxide iron (FeOOH) has a crystal structure containing tunnel-shaped cavities that run parallel to the c-axis. This sites are bound by double rows of fused octahedral in which cadmium ions probably reside.[41]

This is important for understanding that the presence of cadmium ions with FeO and other iron oxides (e.g. $Fe(OH)_2$) is one of the possible interaction that promotes the formation of cadmium ferrite, therefore we propose:

$$2Fe^{2+} + Cd^{2+} + 4OH^- \rightarrow CdFe_2O_4 + 2H_2 \quad (5)$$
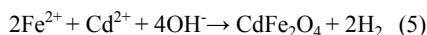
The fiber formation as product of nZVI in the presence of cadmium ions possibly is due to the rearrangement of the nanomaterial structure as a consequence of the adsorption process. Figure 8 shows a schematic of the possible surface reaction.
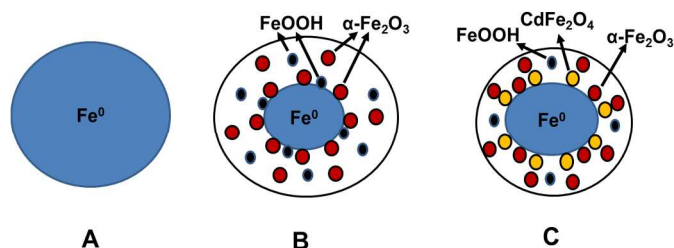

Figure 8. Conceptual model of cadmium adsorption process on nZVI nanostructures with cadmium-iron oxides on the surface.

The interactions of Cd^{+2} and Fe^{+3} particularly, possibly promote the $CdFe_2O_4$ formation which is in accordance with what is reported in the literature [39]. Our results showed the fiber formation as previous studies in the literature with $CdFe_2O_4$ particles synthesized by coprecipitation method[41]. These studies showed the aggregation of fine particles of $CdFe_2O_4$ having two kinds of shapes, fibrous and granular in HRTEM. Due to the fact that XPS and XAS analysis showed that we had the necessary precursors to synthesize $CdFe_2O_4$ in our system and because of the formation of the nanofibrous structures, we can conclude that our remediation process has $CdFe_2O_4$ as a product.

D. Conclusions

nZVI were synthesized using chemical reduction technique and exposed to a Cd-water environment. Accordingly to results obtained in the XPS, XRD and HRTEM techniques, ICP study confirm that cadmium has been removed from water and integrated to the iron oxide after the nZVI treatment. A comprehensive characterization confirmed the production of highly organized nanofibers composed of iron oxides and cadmium ferrite after adding nZVI contact with the cadmium solution. Cd ions were removed from the solution at ca. 90% in 5 hrs by a pH dependent process. Optimum operational pH was identified at a range between 2 and 4. As general overview of the results, hydroxides groups are important to assure the nZVI particles interaction with Cd ions, yet there is a compromise were pH higher than 4 induce a surface passivation that exacerbates when this pH increased. The unintended formation of $CdFe_2O_4$ nanofibers as a remediation product presents an opportunity to reuse the remediation products for applications pertaining to light harvesting.

E. Acknowledgements

Notes and references

[a]University High School, University of Puerto Rico at Río Piedras, San Juan, Puerto Rico 00931
[b]Department of Environmental Sciences, University of Puerto Rico at Río Piedras, San Juan, Puerto Rico, 00931.
[c]Department of Chemistry and Physics, P.O. Box 70377, University of Puerto Rico at Río Piedras, San Juan, Puerto Rico 00936-8377. E-mail: carlos.cabrera2@upr.edu
[d]Physical Sciences Department, University of Puerto Rico at Río Piedras, San Juan, Puerto Rico, 00931.
[e]Physics and Astronomy Department, University of Texas at San Antonio, San Antonio, Texas 78249
[f]Departamento de Ingeniería Química, Universidad de Sonora, 83000 Hermosillo, Sonora, México
[g]School of Environmental Affairs, Metropolitan University, San Juan, Puerto Rico, 00928

(1)	Boparai, H. K.; Joseph, M.; O'Carroll, D. M. *Journal of Hazardous Materials* **2011**, *186*, 458.
(2)	Clemens, S. *Biochimie* **2006**, *88*, 1707.
(3)	Szkoda, J.; Durkalec, M.; Kolacz, R.; Opalinski, S.; Zmudzki, J. *Medycyna Weterynaryjna* **2012**, *68*, 689.
(4)	Castillo-Michel, H. A.; Hernandez, N.; Martinez-Martinez, A.; Parsons, J. G.; Peralta-Videa, J. R.; Gardea-Torresdey, J. L. *Plant Physiology and Biochemistry* **2009**, *47*, 608.
(5)	Babula, P.; Adam, V.; Opatrilova, R.; Zehnalek, J.; Havel, L.; Kizek, R. *Environmental Chemistry Letters* **2008**, *6*, 189.
(6)	Vrinceanu, N.; Motelica, D. M.; Dumitru, M.; Gament, E.; Manea, A.; Tanase, V.; Preda, M. *Scientific Papers, UASVM Bucharest, Series A* **2010**, *LIII*, 73.
(7)	Benavides, M. P.; Gallego, S. M.; Tomaro, M. L. *Brazilian Journal of Plant Physiology* **2005**, *17*, 21.
(8)	Wan, L.; Zhang, H. *Plant Signaling & Behavior* **2012**, *7*, 1.
(9)	McElroy, J. A.; Shafer, M. M.; Trentham-Dietz, A.; Hampton, J. M.; Newcomb, P. A. *Journal of the National Cancer Institute* **2006**, *98*, 869.
(10)	Huff, J.; Lunn, R. M.; Waalkes, M. P.; Tomatis, L.; Infante, P. F. *International Journal of Occupational and Environmental Health* **2007**, *13*, 202.
(11)	*U.S. Environmental Protection Agency. National Center for Environmental Assessment, Office of Research and Development, Washington, DC.* **1999**, http://www.epa.gov/iris/subst/0141.htm.
(12)	Crane, R. A.; Scott, T. B. *Journal of Hazardous Materials* **2012**, *211*, 112.
(13)	Boparai, H. K.; Joseph, M.; O'Carroll, D. M. *Environmental Science and Pollution Research* **2013**, *20*, 6210.
(14)	Kharisov, B. I.; Rasika Dias, H. V.; Kharissova, O. V.; Manuel Jimenez-Perez, V.; Olvera Perez, B.; Munoz Flores, B. *RSC Advances* **2012**, *2*, 9325.
(15)	Adeleye, A. S.; Keller, A. A.; Miller, R. J.; Lenihan, H. S. *Journal of Nanoparticle Research* **2013**, *15*, 18.
(16)	Shipley, H. J.; Engates, K. E.; Guettner, A. M. *Journal of Nanoparticle Research* **2011**, *13*, 2387.

(17)   Ponder, S. M.; Darab, J. G.; Mallouk, T. E. *Environmental Science & Technology* **2000**, *34*, 2564.
(18)   Sun, Y. P.; Li, X. Q.; Cao, J. S.; Zhang, W. X.; Wang, H. P. *Advances in Colloid and Interface Science* **2006**, *120*, 47.
(19)   Bishop, E. J.; Fowler, D. E.; Skluzacek, J. M.; Seibel, E.; Mallouk, T. E. *Environmental Science & Technology* **2010**, *44*, 9069.
(20)   Schrick, B.; Hydutsky, B. W.; Blough, J. L.; Mallouk, T. E. *Chemistry of Materials* **2004**, *16*, 2187.
(21)   Harish, K. N.; Bhojya Naik, H. S.; Prashanth Kumar, P. N.; Vishwanath, R.; Yashvanth Kumar, G. S. *Archives of Applied Science Research* **2013**, *5*, 42.
(22)   Wang, C. B.; Zhang, W. X. *Environmental Science & Technology* **1997**, *31*, 2154.
(23)   Chen, S. Y.; Chen, W. H.; Shih, C. J. *Water Science and Technology* **2008**, *58*, 1947.
(24)   Ravel, B.; Newville, M. *Journal of Synchrotron Radiation* **2005**, *12*, 537.
(25)   Zhang, Y. L.; Li, Y. T.; Dai, C. M.; Zhou, X. F.; Zhang, W. X. *Chemical Engineering Journal* **2014**, *244*, 218.
(26)   Uzum, C.; Shahwan, T.; Eroglu, A. E.; Lieberwirth, I.; Scott, T. B.; Hallam, K. R. *Chemical Engineering Journal* **2008**, *144*, 213.
(27)   Ghods, P.; Isgor, O. B.; Brown, J. R.; Bensebaa, F.; Kingston, D. *Applied Surface Science* **2011**, *257*, 4669.
(28)   Uzum, C.; Shahwan, T.; Eroglu, A. E.; Hallam, K. R.; Scott, T. B.; Lieberwirth, I. *Applied Clay Science* **2009**, *43*, 172.
(29)   Ponder, S. M.; Darab, J. G.; Bucher, J.; Caulder, D.; Craig, I.; Davis, L.; Edelstein, N.; Lukens, W.; Nitsche, H.; Rao, L. F.; Shuh, D. K.; Mallouk, T. E. *Chemistry of Materials* **2001**, *13*, 479.
(30)   Kim, W. B.; Choi, S. H.; Lee, J. S. *The Journal of Physical Chemistry B* **2000**, *104*, 8670.
(31)   Berry, A. J.; O'Neill, H. S. C.; Jayasuriya, K. D.; Campbell, S. J.; Foran, G. J. *American Mineralogist* **2003**, *88*, 967.
(32)   Lee, G. H.; Kim, S. H.; Choi, B. J.; Huh, S. H.; Chang, Y.; Kim, B.; Park, J.; Oh, S. J. *Journal of the Korean Physical Society* **2004**, *45*, 1019.
(33)   Cao, X. B.; Wang, W. H.; Zhang, X. H.; Li, L. Y.; Cheng, Y. H.; Liu, H.; Du, S. C.; Zheng, R. K. *Nanoscale Research Letters* **2013**, *8*.
(34)   Liu, H. B.; Chen, T. H.; Chang, D. Y.; Chen, D.; Liu, Y.; He, H. P.; Yuan, P.; Frost, R. *Materials Chemistry and Physics* **2012**, *133*, 205.
(35)   Fouda, M. F. R.; ElKholy, M. B.; Mostafa, S. A.; Hussien, A. I.; Wahba, M. A.; El-Shahat, M. F. *Advanced Materials Letters* **2013**, *4*, 347.
(36)   Ban, Z. H.; Barnakov, Y. A.; Golub, V. O.; O'Connor, C. J. *Journal of Materials Chemistry* **2005**, *15*, 4660.
(37)   Li, L.; Fan, M. H.; Brown, R. C.; Van Leeuwen, J. H.; Wang, J. J.; Wang, W. H.; Song, Y. H.; Zhang, P. Y. *Critical Reviews in Environmental Science and Technology* **2006**, *36*, 405.
(38)   Chakrabarti, M.; Sanyal, D.; Chakrabarti, A. *Journal of Physics-Condensed Matter* **2007**, *19*.
(39)   Ismail, S. M.; Labib, S.; Attallah, S. S. *Journal of Ceramics* **2013**, *2013*, 8.
(40)   Yehia, M.; Labib, S.; Ismail, S. M. *Physica B-Condensed Matter* **2014**, *446*, 49.
(41)   Yokoyama, M.; Sato, T.; Ohta, E.; Sato, T. *Journal of Applied Physics* **1996**, *80*, 1015.
(42)   Patterson, A. L. *Physical Review* **1939**, *56*, 978.
(43)   Liu, A.; Zhang, W.-x. *Analyst* **2014**.
(44)   Feng, J.; Lim, T. T. *Chemosphere* **2007**, *66*, 1765.
(45)   Ngo, A. T.; Pileni, M. P. *Journal of Physical Chemistry B* **2001**, *105*, 53.
(46)   Liang, W.; Dai, C.; Zhou, X.; Zhang, Y. *Plos One* **2014**, *9*.
(47)   Yan, W. L.; Herzing, A. A.; Kiely, C. J.; Zhang, W. X. *Journal of Contaminant Hydrology* **2010**, *118*, 96.